Inorganic Chemistry

Article

pubs.acs.org/IC

Design and Synthesis of a New Layered Thermoelectric Material $LaPbBiS_3O$

Yun-Lei Sun,[†] Abduweli Ablimit,[†] Hui-Fei Zhai,[†] Jin-Ke Bao,[†] Zhang-Tu Tang,[†] Xin-Bo Wang,[‡] Nan-Lin Wang,[¶,§] Chun-Mu Feng,[†] and Guang-Han Cao*[,†,▽]

[†]Department of Physics, Zhejiang University, Hangzhou 310027, China

[‡]Beijing National Laboratory for Condensed Matter Physics, Institute of Physics, Chinese Academy of Sciences, Beijing 100190, China

[¶]International Center for Quantum Materials, School of Physics, Peking University, Beijing 100871, China

[§]Collaborative Innovation Center of Quantum Matter, Beijing, China

[▽]State Key Lab of Silicon Materials, Zhejiang University, Hangzhou 310027, China

Supporting Information

ABSTRACT: A new quinary oxysulfide $LaPbBiS_3O$ was designed and successfully synthesized via a solid-state reaction in a sealed evacuated quartz tube. This material, composed of stacked NaCl-like $[M_4S_6]$ (where M = Pb, Bi) layers and fluorite-type $[La_2O_2]$ layers, crystallizes in the tetragonal space group $P4/nmm$ with a = 4.0982(1) Å, c = 19.7754(6) Å, and Z = 2. Electrical resistivity and Hall effect measurements demonstrate that it is a narrow gap semiconductor with an activation energy of ∼17 meV. The thermopower and the figure of merit at room temperature were measured to be −52 μV/K and 0.23, respectively, which makes $LaPbBiS_3O$ and its derivatives be promising for thermoelectric applications.

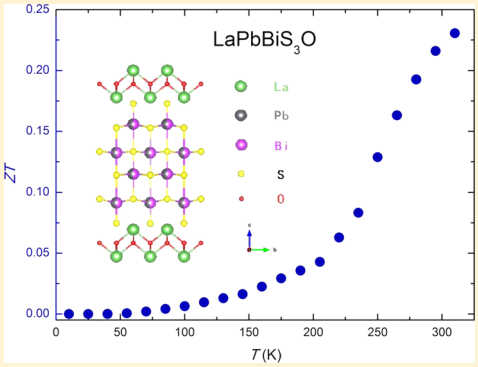

INTRODUCTION

Thermoelectric materials have been studied for many years, since they were demonstrated as a promising solution for power generation as well as energy conversion. Bi_2Te_3-type compounds and their alloys are famous for Peltier application at or below room temperature.[1−3] In the last decades, various systems such as oxides, skutterudites, clathrates, half-Heusler alloys, and PbTe-based materials were found to exhibit good thermoelectric properties.[4−11] Low-dimensional materials may exhibit essential features required for a high figure of merit, because of their anisotropic crystal and electronic structures. For instance, the BiCuXO (X = S, Se, Te) system, with ZrCuSiAs-type layered structure, is of high thermoelectric performance with a maximum figure of merit, $ZT \approx 1.1$, at high temperatures.[12−14] Another layered compound, $CsBi_4Te_6$, achieves a maximum ZT of ∼0.8 at 225 K through suitable doping.[15] Similar materials $CsPbBi_3Te_6$ and $CsPb_2Bi_3Te_7$ were also reported for their large values of thermopower (−50 μV/K and −57 μV/K at 350 K, respectively).[16] These complex Cs−Pb−Bi−Te layered compounds consist of anionic infinite $[M_nTe_{n+2}]$ (M = Pb, Bi; n = 4, 5, 6, 7) slabs separated by the Cs^+ cation layers.[17] Obviously, the infinite $[M_nTe_{n+2}]$ layers are responsible for the large Seebeck coefficient. To explore new thermoelectric materials, it is rational to design a layered compound with the $[M_nTe_{n+2}]$-type slabs.

Recently, a series of BiS_2-based superconductors have attracted much interest, because of their novel superconducting properties.[18−23] The crucial structural unit for superconductivity is $[Bi_2S_4]$ layers, which is isostructural to the $[M_nTe_{n+2}]$ slabs with n = 2. It also contains fluorite-type $[La_2O_2]$ layers. It is remarkable that the undoped parent compound, $LaBiS_2O$, exhibits a large thermopower up to ∼150 μV/K at room temperature.[24] Thus, it is appealing to design a compound containing $[M_nS_{n+2}]$ slabs with $n > 2$, which may be a candidate for thermoelectric materials as well as parent compounds of superconductors. A rational approach is to assemble the two-dimensional (2D) building blocks together, based on the fruitful concept of crystal design.[25−31] In this Article, we report our successful trial on the design and synthesis of a new quinary oxysulfide, $LaPbBiS_3O$, which is composed of stacked $[M_4S_6]$ layers and fluorite-type $[La_2O_2]$ layers. Figure 1 presents how we could design the target compound from these two-dimensional (2D) blocks. The prototype of target compound is LaM_2Te_3O, which consists of stacked $[La_2O_2]$ layers and $[M_4Te_6]$ slabs. After considering lattice match and charge balance, $LaPbBiS_3O$ with a new crystal structure was then designed and finally synthesized. Its physical properties were

Received: July 17, 2014
Published: October 1, 2014

   dx.doi.org/10.1021/ic501687h | Inorg. Chem. 2014, 53, 11125−11129

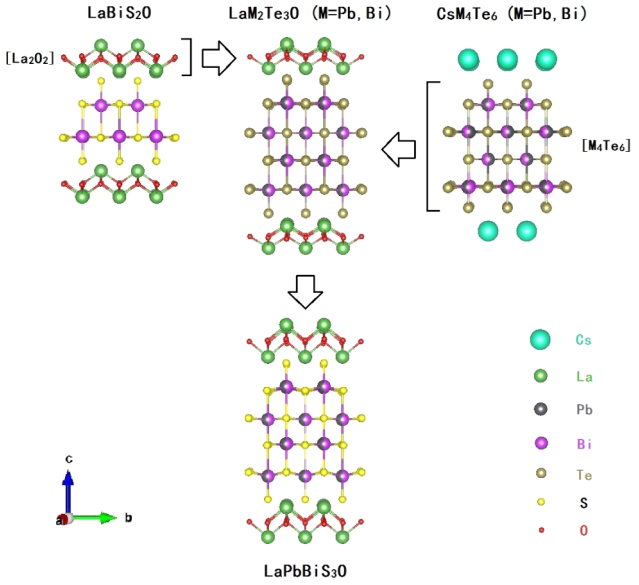

Figure 1. Crystal structure of $LaPbBiS_3O$ designed by hybridization of the two-dimensional (2D) building blocks $[La_2O_2]$ in $LaBiS_2O$ and $[M_4S_6]$ (M = Pb, Bi) in CsM_4Te_6. Lattice match and charge balance were taken into consideration.

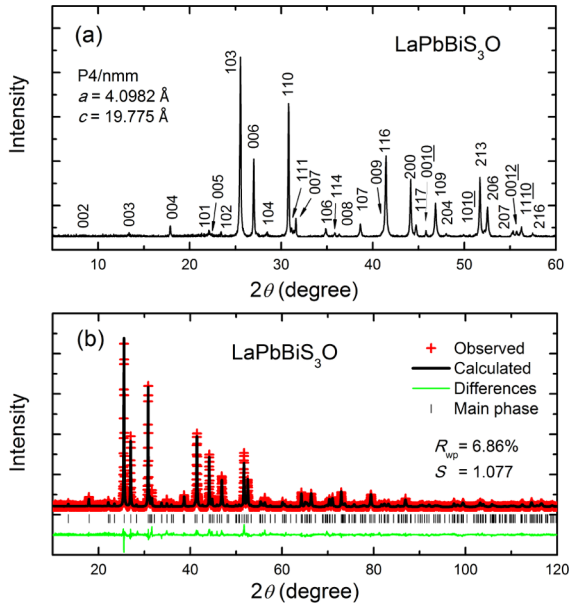

Figure 2. (a) Powder X-ray diffraction (XRD) patterns for $LaPbBiS_3O$ indexed by a tetragonal cell. (b) The Rietveld refinement profile of the XRD pattern for $LaPbBiS_3O$.

then measured, and we conclude that $LaPbBiS_3O$ is a narrow gap semiconductor with a high ZT value, up to 0.23 at room temperature.

EXPERIMENTAL SECTION

Polycrystalline sample of $LaPbBiS_3O$ was synthesized via a solid-state reaction, using high-purity starting materials of La_2S_3, Bi_2S_3 and PbO (Alfa Aesar, ≥99.9%). These starting materials in the stoichiometric ratio were accurately weighed first, and the mixture was placed into an alumina tube, which then was sealed in an evacuated quartz ampule. After that, the ampule was slowly heated to 940 K, holding for 1500 min. The resultant was then ground, pressed into pellets, and sintered under vacuum at 1020 K for another 1500 min, followed by cooling to room temperature. All the operations except for the ampule sealing and heating were carried out in a glovebox with the water and oxygen contents of <1 ppm. The pellet sample obtained was black in color, whose density was measured to be 5.6(1) g/cm^3.

X-ray diffraction (XRD) was performed using a PANalytical diffractometer (Empyrean Series 2) with Cu Kα_1 radiation. The crystal structure at room temperature was refined by Rietveld analysis,[32] and the composition of the polycrystalline samples was checked by a field-emission scanning electron microscopy (SEM) system equipped with an energy-dispersive X-ray spectroscopy (EDX) device. The electrical resistivity was measured on a bar-shaped sample with size of 5.0 mm × 1.7 mm × 1.5 mm by a standard four-terminal method using gold wires and silver paste. We employed a Quantum Design Physical Properties Measurement System (PPMS-9) to measure the Hall coefficient, thermopower, and thermal conductivity in the temperature range of 2−320 K. The infrared diffuse reflectance of polycrystalline $LaPbBiS_3O$ was measured using Bruker spectrometers (Models IFS 113v and 80v) at room temperature. Note that all the measurements of physical properties were performed on the same specimen.

RESULTS AND DISCUSSION

The XRD patterns for $LaPbBiS_3O$ shown in Figure 2a are well-indexed with a tetragonal $P4/nmm$ space group (No.129). No reflections from the possible impurities such as La_2S_3, La_2O_3, Bi_2S_3, and ternary compounds were found. Only few tiny reflections of PbS were observed (the intensity of the strongest impurity peak is <1% of that of the main phase). According to the crystal design described above, the c-axis of $LaPbBiS_3O$ was estimated to be ∼20.0 Å by the formula $c_{LaPbBiS_3O} = c_{LaBiS_2O} + 2 \times d$, where d stands for the interlayer distance in the [BiS] multilayers[20,23] (here, d = 3.1 Å). As expected, the fitted c-axis (19.775 Å) meets the estimated value. Moreover, the fitted a-axis (4.0982 Å) is close to that of $LaBiS_2O$.[20] Therefore, the unit cell coincides with the designed structural model shown in Figure 1.

The detailed structural parameters were obtained by a Rietveld refinement shown in Figure 2b, and the crystallographic data including atomic coordinates are displayed in Table 1. Note that Pb and Bi are assumed to occupy the same crystallographic sites in disorder, and the occupancy were both set to be a fixed value (0.5). One can see that the calculated

Table 1. Crystallographic Data for $LaPbBiS_3O$ Obtained from Powder XRD at Room Temperature

parameter			value		
chemical formula			$LaPbBiS_3O$		
crystal system			tetragonal		
space group			$P4/nmm$ (No. 129)		
unit-cell parameters					
a (Å)			4.0982(1)		
c (Å)			19.7754(6)		
V (Å^3)			332.13(1)		
Z			2		
density (g/cm^3)			6.6724(2)		
atom	site	x	y	z	occupancy
La	2c	0	0.5	0.0852(3)	1.0
O	2a	0	0	0	1.0
Pb/Bi(1)	2c	0.5	0	0.5670(1)	0.5/0.5 (fixed)
Pb/Bi(2)	2c	0.5	0	0.2529(2)	0.5/0.5 (fixed)
S(1)	2c	0.5	0	0.7230(7)	1.0
S(2)	2c	0.5	0	0.4260(9)	1.0
S(3)	2c	0.5	0	0.1236(8)	1.0

dx.doi.org/10.1021/ic501687h | Inorg. Chem. 2014, 53, 11125−11129

profile reproduces the experimental data well. The weighted reliable factor R_{wp} (6.86%) and the goodness-of-fit parameter (1.077) indicate correctness of the designed structure. The quantitative analysis of EDX data collected on platelike crystalline grains (displayed in Table 2) gives the average ratio of La:Pb:Bi:S = 1.00(3):1.08(2):1.07(2):3.15(8) (oxygen content cannot be accurately determined by EDX), which confirms the chemical formula $LaPbBiS_3O$.

Table 2. Energy-Dispersive X-ray (EDX) Data Collected on Crystalline Grains for $LaPbBiS_3O$

	La (at. %)	Pb (at. %)	Bi (at. %)	S (at. %)
1	14.03	14.44	14.86	40.40
2	13.08	14.85	14.16	43.86
3	13.76	14.98	14.71	43.45
average	1.00(3)	1.08(2)	1.07(2)	3.15(8)

The temperature dependence of electrical resistivity $[\rho(T)]$ for $LaPbBiS_3O$ plotted in Figure 3 shows a semiconducting

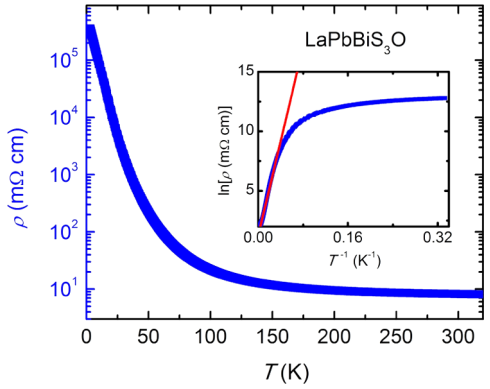

Figure 3. Temperature dependence of electrical resistivity for $LaPbBiS_3O$ from 2 K to 320 K. The inset plots ln ρ vs T^{-1} with an Arrhenius fitting (red line).

behavior with a room-temperature resistivity ρ(300 K) of ~8 mΩ cm. The high-temperature (T = 30–300 K) $\rho(T)$ data obey the thermal activation model,

$$\rho(T) = \rho_0 \exp\left(\frac{E_a}{k_B T}\right)$$

The thermal activation energy E_a was fitted to be ~17.1 meV. In the low-temperature regime (T < 10 K), the data can be fitted by the Mott's law of three-dimensional variable range hopping (VRH) $\rho(T) \propto \exp(T_0/T)^{1/4}$ (not shown here),[33] which suggests the Anderson localization scenario. This means that the activation energy above (E_a) cannot be used to derive the energy band gap. To determine the energy band gap, the infrared diffuse reflectance measurement was performed, and the spectrum is shown in Figure 4. One can see a large drop below 0.1 eV, which may be due to absorption across the band gap. However, it is difficult to determine the band gap value because of the phonon-induced peaklike structure. The band gap can only be roughly estimated to be ~100 meV, according to the reflectance spectrum.

Hall effect measurements under $\mu_0 H$ = 5 T were performed from 2 K to 320 K to identify the species of carriers. The temperature dependence of the Hall coefficient $-R_H(T)$ for $LaPbBiS_3O$ is shown in Figure 5. Consistent with the

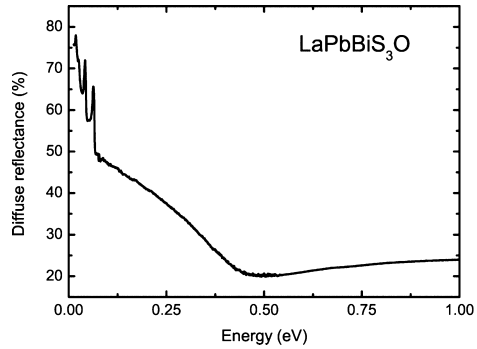

Figure 4. Diffuse reflectance spectrum of polycrystalline $LaPbBiS_3O$ measured at room temperature.

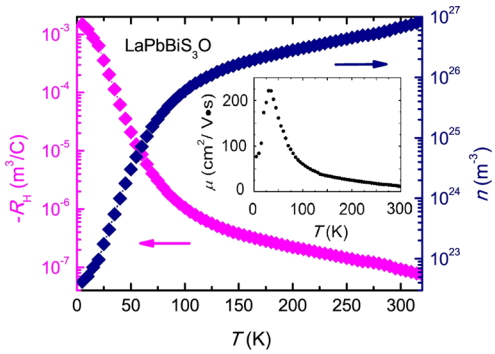

Figure 5. Temperature dependence of Hall coefficient under $\mu_0 H$ = 5 T and carrier concentration for $LaPbBiS_3O$. The inset shows the temperature dependence of carrier mobility.

semiconducting behavior in the $\rho(T)$ curve, the absolute value of Hall coefficient increases by 4 orders of magnitude as temperature decreases. Besides, the negative value of the Hall coefficient for all temperatures indicates that electron carriers dominate, suggesting that the Fermi level is located at the tail of the conduction band (localized states). Taking a single-band picture, the effective carrier concentration was estimated by $n = 1/(eR_H)$ and shown in Figure 5. At room temperature, the carrier concentration is 6.77×10^{26} m^{-3}, which corresponds to 0.05 electrons per Pb/Bi. These carriers are possibly generated due to deviation of stoichiometry. The bismuth content is slightly bit larger than the lead content, because of a small amount of PbS impurity in the sample (such a small deviation cannot be detected by EDX). The decrease in carrier mobility with increasing temperature at high temperatures, shown in the inset of Figure 5, can be understood by phonon scattering. The increase of carrier mobility below 30 K may be associated with the VRH of localized electron carriers, whose mobility is expected to be much lower.

Figure 6a shows the temperature dependence of Seebeck coefficient $S(T)$ for $LaPbBiS_3O$ plotted with black hexagons. One can see that the Seebeck coefficient is negative above 10 K, which confirms that electron carriers dominate the electrical transport. The sign change below 10 K resembles the phenomenon observed in the $SrBiS_2F$ system.[34] This was interpreted by an unknown defect, which induces holelike carriers at low temperatures. With increasing temperature, the absolute value of the Seebeck coefficient increases in a complex manner, which may be related to the Mott's VRH and phonon drag effect. The thermopower achieves a high value of $S \approx -55$ μV/K near room temperature, which is almost the same as that

dx.doi.org/10.1021/ic501687h | Inorg. Chem. 2014, 53, 11125–11129

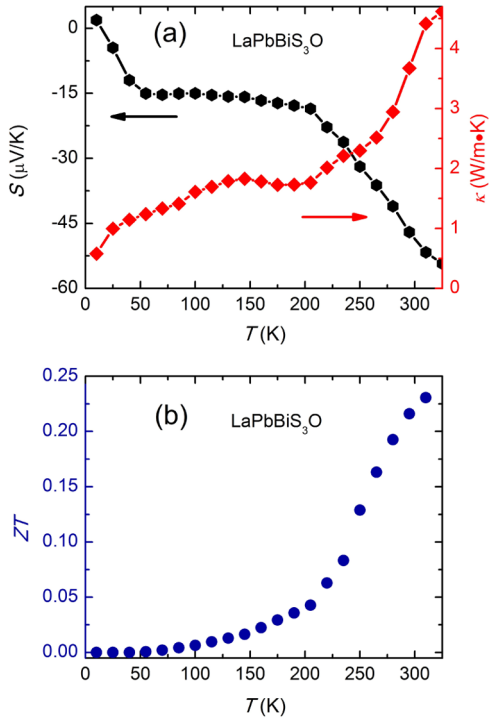

Figure 6. (a) Temperature dependence of thermopower (black hexagons) and thermal conductivity (red squares) at temperatures from 10 K to 320 K for $LaPbBiS_3O$. (b) Temperature dependence of the figure of merit for $LaPbBiS_3O$.

of undoped polycrystalline $CsBi_4Te_6$, $CsPbBi_3Te_6$, and $CsPb_2Bi_3Te_7$,[16,35] but relatively lower than the thermopower of $CsBi_4Te_6$ needles.[15] Previous studies show that the thermoelectric properties of $CsBi_4Te_6$ are strongly dependent on crystalline directions, and relatively lower S values are ascribed to the random orientation of the grains.[35] This implies that growing single crystals of $LaPbBiS_3O$ might significantly improve its thermopower.

Thermal conductivity $\kappa(T)$ was also measured for $LaPbBiS_3O$ as plotted with red squares in Figure 6a. The $\kappa(T)$ value is comparable to that of $CsBi_4Te_6$ system.[15,16,35,36] Generally, thermal conductivity (κ) can be described by the formula

$$\kappa = \kappa_{latt} + \kappa_{ele}$$

where κ_{latt} stands for lattice contribution, while κ_{ele} is the carrier contribution. The lattice thermal conductivity can be described by

$$\kappa_{latt} = \left(\frac{1}{3}\right) C_V l v_s$$

where C_V is the specific heat at constant volume, l the mean free path, and v_s the average velocity of sound. At low temperatures, κ_{ele} is negligible (even at room temperature, κ_{ele} has a value of only ~0.1 W/(m K)), because of the low electrical conductivity according to Wiedemann–Franz law, while the behavior of κ_{latt} is dominated by the linear relation with C_V. Therefore, κ increases at low temperature, as shown in Figure 6a. As the temperature increases, the lattice thermal conductivity is dominated primarily by phonon–phonon scattering, which makes κ decrease from a temperature of 150 K to a temperature of 200 K. The increase of κ at T > 200 K could be ascribed to the contribution of the Pb/Bi disorder-induced glass state. The thermal conductivity of glass is substantially smaller at low temperatures, and it tends to increase with temperature almost monotonically.[37] As a result, κ increases over almost in the entire temperature range and tends to be ~4 W/(m K) at room temperature. It is expected that doping heavy elements in $LaPbBiS_3O$ is a rational approach to reduce the lattice thermal conductivity, since κ_{latt} is approximatively proportional to $\rho^{2/3}/A^{7/6}$ (ρ and A denote the density and the mean atomic weight, respectively).[4] Besides, nanostructuring this material may also minimize the thermal conductivity.[4,38]

ZT, which is a dimensionless figure of merit to characterize thermoelectric materials, is defined as

$$ZT = \frac{S^2 \sigma T}{\kappa}$$

where $\sigma = 1/\rho$ is the electrical conductivity. As shown in Figure 6b, ZT increases rapidly above 250 K and reaches a value of 0.23 around room temperature, comparable with some optimized $CsBi_4Te_6$ specimens.[36,39] Although the high-temperature ZT data were not measured due to limitations of our experimental conditions, they tend to increase further above room temperature. We expect that the thermoelectric properties could be further improved by minimization of κ_{latt}, and by improvement of the Seebeck coefficient, as discussed above.[40]

To summarize, a new quinary oxysulfide $LaPbBiS_3O$ containing $[(Pb,Bi)_4S_6]$ layers was designed and successfully synthesized. Electrical resistivity and Hall effect measurements demonstrate that it is a narrow gap semiconductor. Thermopower and thermal conductivity measurements show that the material exhibits a considerably high figure of merit (0.23) at room temperature. Further optimization of the thermoelectric properties is very promising. Besides, superconductivity might also be introduced by tuning the carrier concentration and by reducing the disorder effect.

■ ASSOCIATED CONTENT

Supporting Information

This material is available free of charge via the Internet at http://pubs.acs.org.

■ AUTHOR INFORMATION

Corresponding Author

*E-mail: ghcao@zju.edu.cn.

Notes

The authors declare no competing financial interest.

■ ACKNOWLEDGMENTS

This work was supported by Scholarship Award for Excellent Doctoral Student granted by Ministry of Education, NSF of China (Grants No. 11190023), the National Basic Research Program of China (Grant Nos. 2010CB923003 and 2011CBA00103), and the Fundamental Research Funds for the Central Universities of China (Grant No. 2013FZA3003).

■ REFERENCES

(1) Testardi, L. R.; Bierly, J. N., Jr.; Donahoe, F. J. *J. Phys. Chem. Solids* **1962**, *23*, 1209–1217.
(2) Kim, W.; Rosi, F. *Solid-State Electron.* **1972**, *15*, 1121–1134.
(3) Venkatasubramanian, R.; Siivola, E.; Colpitts, T.; O'Quinn, B. *Nature* **2001**, *413*, 597–602.
(4) Sootsman, J. R.; Chung, D. Y.; Kanatzidis, M. G. *Angew. Chem., Int. Ed.* **2009**, *48*, 8616–8639.
(5) Snyder, J. G.; Toberer, E. S. *Nat. Mater.* **2008**, *7*, 105–114.

(6) Terasaki, I.; Sasago, Y.; Uchinokura, K. *Phys. Rev. B* **1997**, *56*, R12685−R12687.
(7) Itahara, H.; Tani, T. *R&D Rev. Toyota CRDL* **2004**, *39*, 63−70.
(8) Ren, Z.; Shen, J.-Q.; Jiang, S.; Chen, X.-Y.; Feng, C.-M.; Xu, Z.-A.; Cao, G.-H. *J. Phys.: Condens. Matter* **2006**, *18*, L379−L384.
(9) Zhao, L.-D.; Lo, S.-H.; Zhang, Y.; Sun, H.; Tan, G.; Uher, C.; Wolverton, C.; Dravid, V. P.; Kanatzidis, M. G. *Nature* **2014**, *508*, 374−377.
(10) Kimmel, J. *Thermoelectric Materials*; Special Topic Paper for Physics 152, 1999.
(11) Goncalves, A. P.; Godart, C. *Eur. Phys. J. B* **2014**, *87*, 42−71.
(12) Zhao, L. D.; Berardan, B. D.; Pei, Y. L.; Byl, C.; Pinsard-Gaudart, L.; Dragoe, N. *Appl. Phys. Lett.* **2010**, *97*, 092118.
(13) Kusainova, A.; Berdonosov, P.; Akselrud, L.; Kholodkovskaya, L.; Dolgikh, V.; Popovkin, B. *J. Solid State Chem.* **1994**, *112*, 189−191.
(14) Li, J.; Sui, J.; Pei, Y.; Barreteau, C.; Berardan, D.; Dragoe, N.; Cai, W.; He, J.; Zhao, L.-D. *Energy Environ. Sci.* **2012**, *5*, 8543−8547.
(15) Chung, D. Y.; Hogan, T.; Brazis, P.; Rocci-Lane, M.; Kannewurf, C. R.; Bastea, M.; Uher, C.; Kanatzidis, M. G. *Science* **2000**, *287*, 1024−1027.
(16) Hsu, K.-F.; Chung, D.-Y.; Lal, S.; Mrotzek, A.; Kyratsi, T.; Hogan, T.; Kanatzidis, M. G. *J. Am. Chem. Soc.* **2002**, *124*, 2410−2411.
(17) Hsu, K.-F.; Chung, D.-Y.; Lal, S.; Hogan, T.; Kanatzidis, M. G. *Mater. Res. Soc. Symp. Proc.* **2002**, *691*, G8.25.1−G8.25.6.
(18) Mizuguchi, Y.; Fujihisa, H.; Gotoh, Y.; Suzuki, K.; Usui, H.; Kuroki, K.; Demura, S.; Takano, Y.; Izawa, H.; Miura, O. *Phys. Rev. B* **2012**, *86*, 220510.
(19) Xing, J.; Li, S.; Ding, X.; Yang, H.; Wen, H.-H. *Phys. Rev. B* **2012**, *86*, 214518.
(20) Mizuguchi, Y.; Demura, S.; Deguchi, K.; Takano, Y.; Fujihisa, H.; Gotoh, Y.; Izawa, H.; Miura, O. *J. Phys. Soc. Jpn.* **2012**, *81*, 114725.
(21) Awana, V.; Kumar, A.; Jha, R.; Singh, S. K.; Pal, A.; Shruti; Saha, J.; Patnaik, S. *Solid State Commun.* **2013**, *157*, 21−23.
(22) Usui, H.; Suzuki, K.; Kuroki, K. *Phys. Rev. B* **2012**, *86*, 220501.
(23) Yildirim, T. *Phys. Rev. B* **2013**, *87*, 020506.
(24) Omachi, A.; Kajitani, J.; Hiroi, T.; Miura, O.; Mizuguchi, Y. *J. Appl. Phys.* **2014**, *115*, 083909.
(25) Cario, L.; Kabbour, H.; Meerschaut, A. *Chem. Mater.* **2005**, *17*, 234−236.
(26) Ferey, G. *J. Solid State Chem.* **2000**, *152*, 37−48.
(27) Yaghi, O. M.; O'Keeffe, M.; Ockwig, N. W.; Chae, H. K.; Eddaoudi, M.; Kim, J. *Nature* **2003**, *423*, 705−714.
(28) Sun, Y.-L.; Jiang, H.; Zhai, H.-F.; Bao, J.-K.; Jiao, W.-H.; Tao, Q.; Shen, C.-Y.; Zeng, Y.-W.; Xu, Z.-A.; Cao, G.-H. *J. Am. Chem. Soc.* **2012**, *134*, 12893−12896.
(29) Jiang, H.; Sun, Y.-L.; Xu, Z.-A.; Cao, G.-H. *Chin. Phys. B* **2013**, *8*, 087410.
(30) Mrotzek, A.; Kanatzidis, M. G. *Acc. Chem. Res.* **2003**, *36*, 111−119.
(31) Kanatzidis, M. G. *Acc. Chem. Res.* **2005**, *38*, 361−370.
(32) Izumi, F.; Ikeda, T. *Mater. Sci. Forum* **2000**, *321*−*324*, 198−205.
(33) Mott, N. F. *Philos. Mag.* **1968**, *17*, 1259−1267.
(34) Lei, H.; Wang, K.; Abeykoon, M.; Bozin, E. S.; Petrovic, C. *Inorg. Chem.* **2013**, *52*, 10685−10689.
(35) Datta, A.; Nolas, G. S. *ACS Appl. Mater. Interfaces* **2012**, *4*, 772−776.
(36) Chung, D.-Y.; Hogan, T. P.; Rocci-Lane, M.; Brazis, P.; Ireland, J. R.; Kannewurf, C. R.; Bastea, M.; Uher, C.; Kanatzidis, M. G. *J. Am. Chem. Soc.* **2004**, *126*, 6414−6428.
(37) Yang, J. In *Thermal Conductivity: Theory, Properties, and Applications*; Tritt, T. M., Ed.; Springer: New York, 2004; Chapter 1.1.
(38) Son, J. S.; Choi, M. K.; Han, M.-K.; Park, K.; Kim, J.-Y.; Lim, S. J.; Oh, M.; Kuk, Y.; Park, C.; Kim, S.-J.; Hyeon, T. *Nano Lett.* **2012**, *12*, 640−647.
(39) Chung, D. Y.; Uher, C.; Kanatzidis, M. G. *Chem. Mater.* **2012**, *24*, 1854−1863.
(40) Xiao, C.; Li, Z.; Li, K.; Huang, P.; Xie, Y. *Acc. Chem. Res.* **2014**, *47*, 1287−1295.